Hindawi
Advances in Civil Engineering
Volume 2021, Article ID 6690171, 16 pages
https://doi.org/10.1155/2021/6690171

Research Article

Impact of Moisture Content on the Brittle-Ductile Transition and Microstructure of Sandstone under Dynamic Loading Conditions

Aihong Lu,[1,2] **Xiya Chang**,[1,2] **Shanchao Hu**,[3] **Yu Xia**,[1,2] **and Ming Li**[1,2]

[1]*State Key Laboratory for Geomechanics and Deep Underground Engineering, China University of Mining &Technology, Xuzhou 221116, China*
[2]*School of Mechanics and Civil Engineering, China University of Mining & Technology, Xuzhou 221116, China*
[3]*China Coal Technology and Engineering Group Chongqing Research Institute, Chongqing 400039, China*

Correspondence should be addressed to Aihong Lu; xzlah@126.com

Received 17 December 2020; Accepted 22 April 2021; Published 5 May 2021

Academic Editor: Hualei Zhang

Rockburst frequently occurred in an unstable or violent manner, which posed great safety risk and economic loss in deep underground engineering. The water injection into rock stratum was one of the most effectively ways to reduce rockburst by weakening rock mechanics. However, the moisture content was an important index related to rock mechanical properties. Many previous studies focused on the relationship between the moisture contents and macromechanical properties of rock materials under static load and seldom explored the impact of moisture variation on the mechanical properties and brittle-ductile transition characteristics of rock materials under dynamic loads. In this paper, we studied the dynamic mechanical properties of sandstone with different moisture contents under the same strain rate by the Split Hopkinson Pressure Bar (SHPB) experimental system. The relationship between dynamic mechanical properties of sandstone and moisture content was studied, and a dynamic ductility coefficient was proposed, which could be determined by the ratio between the peak strain and the yield strain. Then, it was used to assess the critical moisture content of the brittle-ductile transition of the sandstone. Through scanning electron microscopy (SEM) examination, the microstructure of sandstones with different moisture contents was inspected at magnifications of 500, 2000, and 5000 times, respectively. We showed that as the moisture content increased, the dynamic peak strength and elastic modulus decreased at different degrees, whereas the dynamic peak strain and ductility coefficient exhibited a nonlinear increase, respectively. When the moisture content reached 2.23%, the variation ratio of the dynamic ductility coefficient commenced to increase obviously, indicating that the sandstone began to transit from brittle behavior to ductile behavior. When the sample magnification was 500 times, the microstructure of the sandstone samples with zero and 2.01% to 2.40% moisture content mainly displayed the step pattern and river pattern, respectively, showing that the damage mode was brittle fracture. When the moisture content ranged from 2.49% to 2.58%, the microstructure of the sample included a large number of dimple clusters with local snake patterns and belonged to ductile fracture. When the sample magnification was 2000 and 5000 times, the microstructure was mainly brittle fracture with a moisture content lower than 2.23%. The microstructure of the sample with moisture content of 2.23% exhibited brittle-ductile composite fracture form, whereas others exhibited obviously ductile fracture. These characteristics were fundamentally consistent with the results reflected by the dynamic ductility coefficient. Our findings could provide a theoretical basis for mitigating coal and rock bursts by injecting water methods in underground coal mines.

1. Introduction

The strength and deformation of rock materials was crucially affect by water, which was a key factor inducing major geological disasters such as landslides, karst collapses, and water inrush (Iverson [1] and Bai [2]). Investigating the effect of moisture content on rock strength and deformation was critical to prevention and control of the abovementioned disasters. On the other hand, with the rapid development of China's economy, increasing rock-engineering projects were exposed to dynamic loadings, such as blasting excavation of roadways and tunnels, oil and gas drilling, and coal and rock

bursts (Lu [3], Song [4], Zhang [5], and Zhao [6]). Therefore, in-depth understanding of the dynamic mechanical properties and the brittle-ductile evolution of rocks with different moisture contents offered theoretical foundation for practical rock-engineering design.

Many scholars have carried out studies on the effect of moisture content on static/dynamic mechanical and brittle-ductile properties of rocks based on uniaxial/triaxial compression tests and creep tests. Under static load conditions, previous work could be summarized as follows: (1) the static compressive strength and elastic modulus of the sample decreased as the moisture content increased (Wasantha [7] and Zhang [8]). (2) Water effectively reduced the rock brittleness by 5%~17% and enhanced its ductility (Baud [9], Liu [10], Nicolas [11], Fujimoto [12], Zhu [13], Han [14], Duba [2], Suppe [15], and Han [14]). For example, Liu et al. (Liu and Shao [16]) performed compressive tests on four clay rocks with different humidity under the constant strain condition and found that the peak and residual strength of the clay rock gradually decreased with the increase of moisture content, whereas the ductility was gradually enhanced. However, there was no approach to quantify the ductile features. Wong et al. [17] found that the weakening effect of water on different types of rocks was quite different. As the moisture content increased, the uniaxial compressive strength of quartzite was nearly unvaried, whereas the uniaxial compressive strength of shale was reduced by 90%. Under impact load conditions, Kim et al. (Kim and De [18]) studied the dynamic peak stress of sandstones with different pore sizes under dry and saturated conditions and reported that the dynamic peak strength of dry sandstone was the highest. Zhou and Kim et al. (Zhou [19] and Kim [20]) compared the mechanical properties of rock specimens under dry and saturated conditions subjected to dynamic loading. It was found that the specimen compressive strength under saturated state was significantly lower than that of the dry state, but in-depth explanation on the brittle-ductile transition of the specimen was still absent. Wong et al. (Wong and Baud [21]) also explained the promotion of water on the brittle-ductile transition of rock.

Existing studies have reported that water was one of the important factors affecting the physical and mechanical properties of rocks. Quantitative study on the brittle-ductility of rock was mainly represented by the brittle-ductility coefficient. The coefficient mainly considers the following four aspects (Kahraman [22], Altindag [23], Kahraman [24], Gong [25], Tarasov [26], and Tarasov [27]), i.e., energy ratio or energy increment ratio method, rock strength (compressive strength and tensile strength, etc.) comparison method, using the rock cutting speed to reflect the brittleness, and selecting 80% of the peak strain as its ductility coefficient to reflect the rock ductility. The above methods only consider the influence of static load on the brittle-ductility of rock, and its applicability under dynamic load conditions remains uncertain.

The microscopic morphology of sandstone was the intrinsic manifestations of macroscopic failure. The observation of rock fracture morphology by scanning electron microscopy (SEM) was widely used to study the brittle-ductile transition of rock. Zhang et al. (Zhang [28]) studied the influence of temperature on the brittle-ductile transition of rock based on the mesomorphological characteristics through SEM and determined the critical temperature of the brittle-ductile transition. Frances et al. (Cooper, Platt, and Behr [29]) obtained two different transiting modes during brittle-ductile transitions of crust rock through microstructure analysis and thermal-physical measurement data. Zhou et al. (Zhou, He, and Yang [30]) studied the micromorphology and fracture of mafic ore and reported that water posed a significant impact on the brittle-ductile transition of mafic ore.

Most existing studies have compared the mechanical properties of dry and saturated samples. It was rare to disclose the effect of moisture content on the dynamic brittle-ductile transition of rock. In this paper, the influence of moisture content on the dynamic mechanical properties of sandstone was analyzed and a dynamic ductility coefficient was defined. The relationship between the dynamic ductility coefficient and the moisture content was quantitatively established from a macroscopic viewpoint. The microfracture morphology of the specimen after dynamic loading was examined by SEM. The relationship between the brittle-ductile transition and the moisture content was further revealed microscopically. The findings could provide significant guidance for revealing the mechanism of water mitigating the occurrence of rock burst in rock-engineering projects.

2. Experimental Study

2.1. Sample Preparation. The red sandstone (Figure 1) used in the test was relatively homogenous without obvious joints. The cylindrical sample was sized 50×50 mm (diameter-$\times$height). The 50 mm diameter sample was drilled by a coring machine, followed by cutting into standard specimens with a height of 50 mm. A double-sided sander was used to polish both sides of the flat surface less than 0.05 mm and end parallelism less than 0.02 mm. To reduce the effect of sample heterogeneity on the experimental results, the longitudinal wave velocity of the sample was fist examined. The sample with a wave velocity of approximately 3400 ($\pm$25) m/s was selected for testing. The physical and mechanical properties of the standard sandstone samples under static loading were obtained by uniaxial compression and in-direct tension tests. The test results are shown in Table 1. The measurements listed in the table were the average values of five samples.

2.2. SHPB System

2.2.1. Experimental System. We employed a 50 mm diameter Split Hopkinson Pressure Bar (SHPB) test system to perform the experiments. The simplified structure is shown in Figure 2. The whole system included the loading-drive system, the pressure bar system, the energy absorption system, the signal acquisition system, and the signal processing system. The sample was sandwiched between the incident rod and the transmission rod. During the test, the high-pressure gas pushed the impact rod to collide with the incident bar and generated a pulse stress wave at the

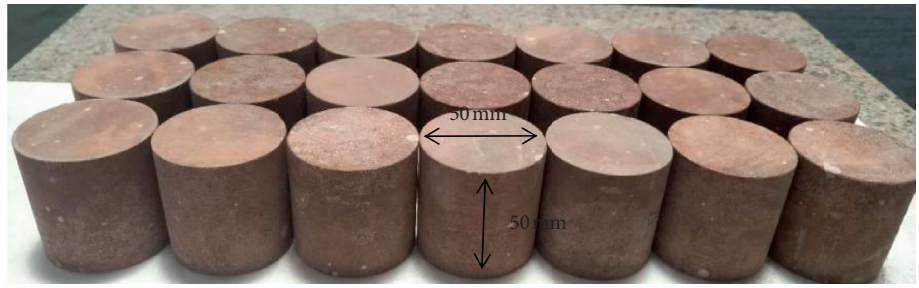

Figure 1: Sandstone samples for experiments.

Table 1: Physical-mechanical properties of the sandstone (note: E is the elastic modulus; ρ and μ are, respectively, density and Poisson ratio; σ_c and σ_t are uniaxial compressive and tensile strength, respectively).

E (GPa)	σ_c (MPa)	ρ (kg/m^3)	σ_t (MPa)	M
7.13	119.88	2120	3.37	0.13

interface between the impact rod and the incident rod. The stress wave propagated along the incident rod to the sample and interfaces with the rod at both ends of the sample. Multiple reflections and refractions were formed at the site, causing high-speed deformation and destruction of the sample. At the same time, part of the stress wave was reflected back into the incident rod, and the other part was propagated into the transmission rod to form reflected waves and transmitted waves, respectively. The strain signal of the incident rod and the transmission rod could be collected into the data acquisition system through the strain gauge, and then the three-wave method was used to process the strain signal of the rod to obtain the force and deformation data of the specimen during the impact test.

2.2.2. Experimental Principle. Based on the one-dimensional stress wave transfer theory and the stress uniformity assumption, the stress, strain, and strain rate of the specimen could be expressed by incident wave, reflected wave, and transmitted wave, respectively. The specific expression was as follows (Ma and Yao [31]):

$$\begin{cases} \dot{\varepsilon} = \dfrac{C_S}{l}\left[\varepsilon_i(t) - \varepsilon_r(t) - \varepsilon_t(t)\right], \\ \varepsilon = \dfrac{C_S}{l}\displaystyle\int_0^t \left[\varepsilon_i(t) - \varepsilon_r(t) - \varepsilon_t(t)\right]dt, \\ \sigma = \dfrac{A_S}{2A_0}E_0\left[\varepsilon_i(t) + \varepsilon_r(t) + \varepsilon_t(t)\right], \end{cases} \tag{1}$$

where $\dot{\varepsilon}$ is the average strain rate in the specimen; C_s is the wave velocity of the stress wave in the rod; $\varepsilon_i(t)$, $\varepsilon_r(t)$, and $\varepsilon_t(t)$, respectively, represent the strain signals of the incident wave, the reflected wave, and the transmitted wave; l represents the original length of the sample; σ and ε are the stress and strain of the sample, respectively; A_s and A_0, respectively, denote the cross-sectional areas of the rod the specimen; and E_0 is the elastic modulus of the rod.

According to the stress uniformity assumption, if the stresses in the sample are equal, we have

$$\varepsilon_i(t) + \varepsilon_r(t) = \varepsilon_t(t). \tag{2}$$

Substituting equation (2) into equation (1), the stress-strain relationship of the sample in the SHPB test is

$$\begin{cases} \dot{\varepsilon} = -2\dfrac{C_s}{l}\varepsilon_r(t), \\ \varepsilon = -2\dfrac{C}{l}\displaystyle\int_0^t \varepsilon_r(t)dt, \\ \sigma = \dfrac{A_s}{A_0}E_0\varepsilon_t(t). \end{cases} \tag{3}$$

2.3. Experimentation

2.3.1. Moisture Content Determination. The sample was placed in an oven, continuously dried at 105°C for 24 hours and weighed. Then, the sample was dried at this temperature for 1 hour for second-time weighing. If the weight difference was less than 0.01 g, we considered the sample to be completely dried. If the difference was greater than 0.01 g, the above process was repeated until the difference of the two adjacent weighing results was less than 0.01 g. All the dried samples were placed in a constant-temperature oven for storage. The dried sample was placed in a transparent glass containing fresh water to completely immerse the sample, and the mass was measured per hour and the moisture content was calculated. Through the above process, seven groups of sandstone samples with different moisture contents (i.e., 0%, 2.01%, 2.23%, 2.40%, 2.49%, 2.53%, and 2.58%) were obtained, and each group of samples contained 10 samples. The sandstone moisture content is

$$\omega = \frac{m_a - m_d}{m_d} \times 100\%, \tag{4}$$

where ω is the moisture content of the sandstone, m_a is the mass after the sample is immersed, and m_d is the mass of the dry sample.

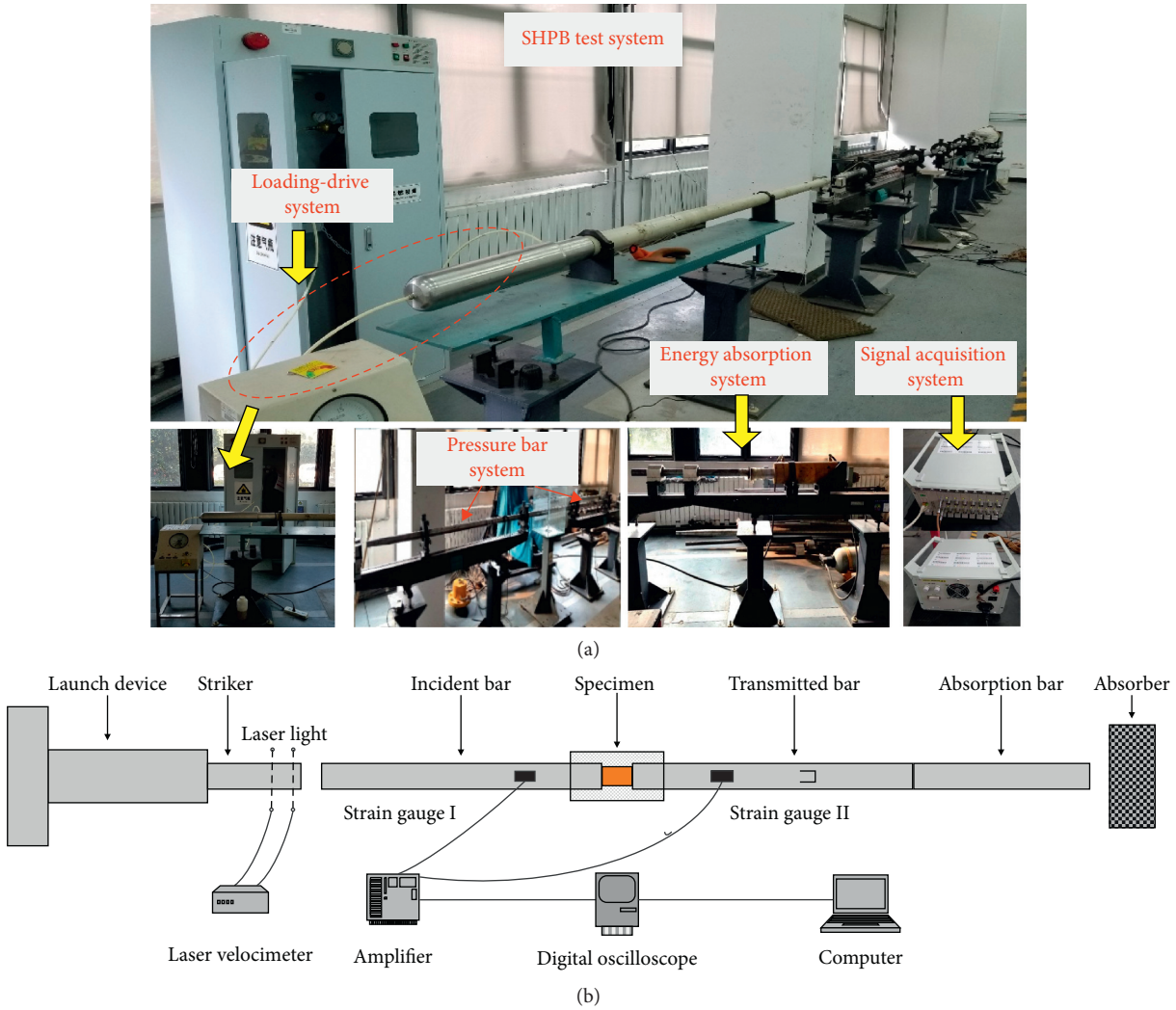

Figure 2: Illustration of the SHPB experimental system: (a) SHPB real products; (b) SHPB structural diagram.

2.3.2. SHPB Test. The loading pressure was determined at 0.25 MPa through the preliminary test. Then, the SHPB system was used to conduct impact test on the seven groups of sandstone samples with different moisture contents (i.e., 0%, 2.01%, 2.23%, 2.40%, 2.49%, 2.53%, and 2.58%). To reduce the effect of the strain rate, three samples with relatively close strain rates were selected to study the brittle-ductility transition law of sandstone in each sample group. The strain rate of the specimen obtained in this impact test was 85 (±5) s^{-1}, which ensured the reliability of the test results.

2.3.3. Optimization of Waveform Shaper. To ensure that the SHPB system satisfied the one-dimensional stress wave transfer theory, the rubber wave shaper was used to adjust the stress wave waveform during the test. Research showed that the waveform shaper has obvious size effect (Yan and Chen [32]). The rubber shaper sizes with the diameter of 5 mm, 10 mm, and 15 mm and thickness of 3 mm were tested at the impact pressure of 0.25 MPa. Every rubber shaper was struck three to five times, and the typical stress wave shapes of different waveform shapers are shown in Figure 3.

Figure 3 shows that when a rubber shaper with a diameter of 5 mm was used, the obtained waveform had the largest amplitude, the shortest wavelength, and the steepest waveform. It means that the sample would reach its peak strength in a very short time during impact test. At this time, the stress inside the sample had not reached the uniform state. Hence, the stress uniformity hypothesis was not satisfied. When a rubber shaper with a diameter of 15 mm was used, the amplitude of the waveform was the smallest, but because the wavelength was too long, the incident wave of the waveform and the reflected wave partially overlap, and the waveform could not be separated and calculated; in addition, when a 10 mm waveform shaper was used, the waveform was gentle and the segmentation was clear, and the performance was a typical semisinusoidal type. Therefore, it was more reasonable to select a rubber sheet with a diameter of 10 mm as a waveform shaper in this test. In addition, to eliminate the friction effect of the end face, it was necessary to apply an appropriate amount of lubricant at the interface between the sample and the rod. Figure 4 shows the typical waveforms of sandstone in the SHPB test.

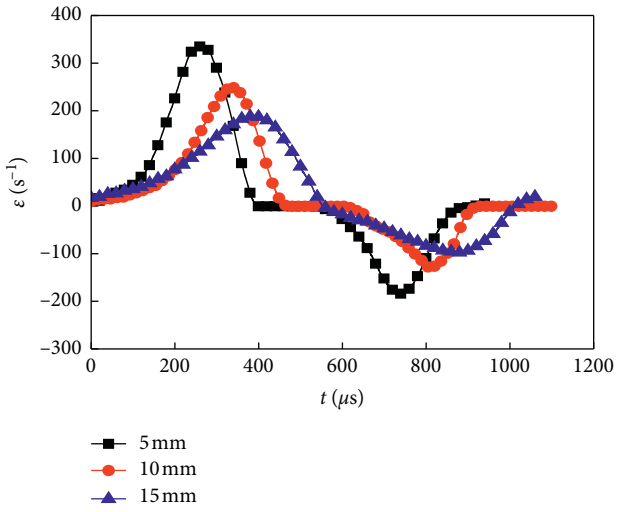

Figure 3: Influence of waveform shaper diameter on waveform.

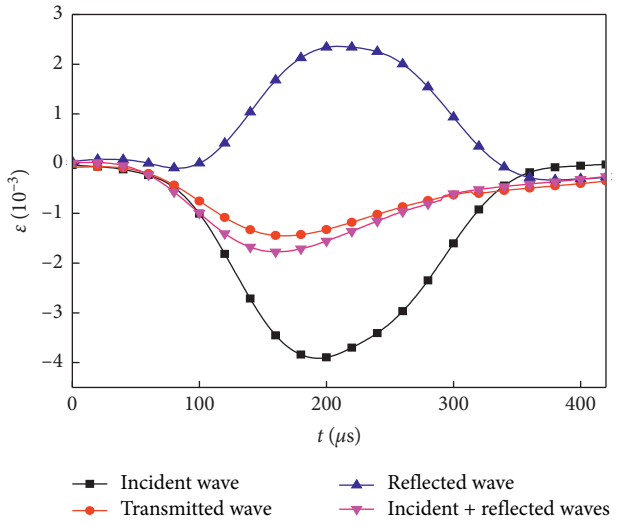

Figure 4: Typical waveform of the SHPB results of the sandstone.

Figure 4 shows that the incident wave was approximately semisinusoidal and had no significant lateral vibration, satisfying the one-dimensional propagation assumption of the stress wave. Both the incident wave and the reflected wave exhibited a slowly rising and then gradually decreasing characteristic with increasing time. The incident wave and the reflected wave reached the peak strain at 200 μs and the sum of them was approximately equal to the transmitted wave, indicating that the stress uniformity assumption was satisfied (Li [33]).

3. The Dynamic Mechanical Properties of Sandstone with Different Moisture Contents

3.1. Effect of Moisture Content on the Dynamic Stress-Strain Curve of Sandstone. After the impact test, the experimental results were processed by the two-wave method, and the dynamic stress-strain curves of the sandstone samples with different moisture contents were plotted (Figure 5). Figure 6 presents the typical stress-strain curve of the test. Clearly, the sandstone sample had undergone five stages under impact, namely, a nonlinear elastic compression stage, a linear elastic stage, a crack nonlinear expansion stage, a postpeak compression stage, and a stress unloading stage. In the nonlinear elastic stage, the original microcracks and voids in the specimen were gradually compressed until they were completely closed. At this time, the elastic modulus increased nonlinearly, and the increasing rate gradually grew preceding entering the linear elasticity stage. In the compression stage, few new cracks initiate inside the sample, and the relationship of stress-strain curve were approximately linear. As the sample continues to be compressed, the internal maximum stress gradually exceeded the crack initiation stress, and new microcracks began to be produced and gradually expanded; the sample entered the plastic yield stage. When the sample arrived its ultimate compressive strength, it began to enter the postpeak compression stage and the stress unloading stage, at which the internal microcracks of the sample had penetrated to the surface and formed macroscopic cracks. The resistance to deformation was drastically reduced until they were completely broken.

Figure 7 shows the dynamic stress-strain curves of sandstone with different moisture contents. According to Figure 7, the following statements could be summarized:

(1) At any moisture content, the sandstone sample experienced obvious nonlinear elastic compression stage. As the moisture content gradually increased, the whole nonlinear elastic compression stage gradually expanded. It was the shortest for the dry sample.

(2) At any moisture content, the sandstone sample exhibited obvious postpeak strain softening stage. When the moisture content was in the range of 0%~2.23%, the stress-strain curve in the postpeak compression stage exhibited dramatically stress drop characteristics. When the moisture content varied from 2.40% to 2.58%, the postpeak stress-strain curve decreased slowly, indicating that when the moisture content reached 2.40%, the ductility of the sample increased significantly.

(3) The moisture content affected significantly the deformation and strength of sandstone samples. That was, the yield strength, elastic modulus, peak strain, and peak strength of the samples changed significantly with the increase of the moisture content (Table 2).

3.2. Effect of Moisture Content on the Dynamic Elastic Modulus of Sandstone. Figure 8 shows the dynamic elastic modulus of sandstone samples as a function of moisture content. In general, there were many various methods to determine elastic modulus, which mainly included secant modulus, tangent modulus, average modulus, and so on. In this work, we took the straight-line slope of the stress-strain curve in elastic stage as the elastic modulus of the specimen. The methods have already been used in other papers [33].

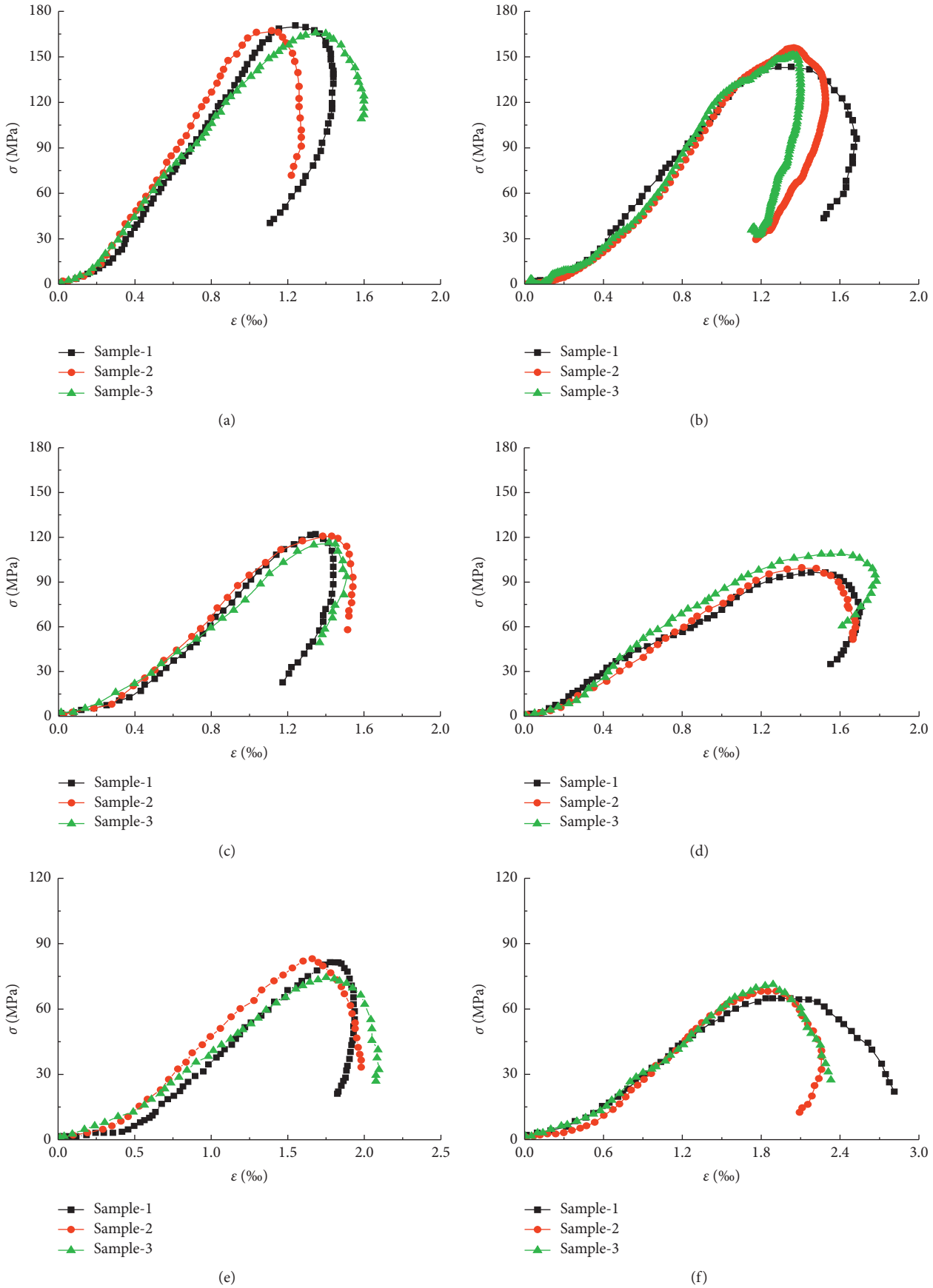

Figure 5: Continued.

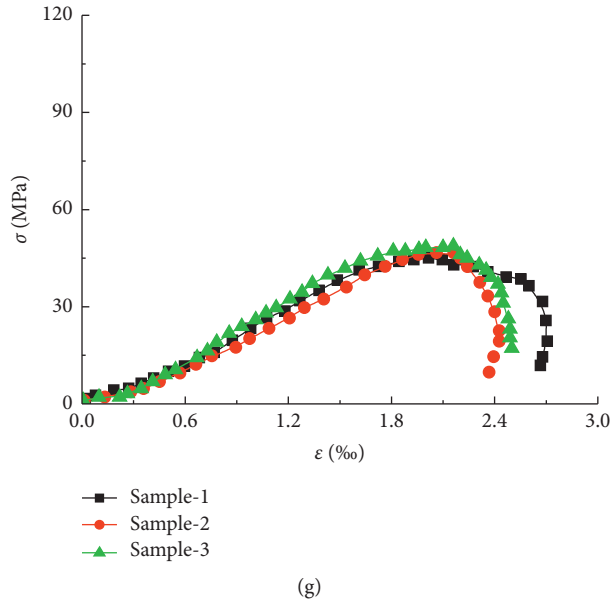

(g)

Figure 5: Stress-strain curves of samples with different moisture contents under dynamic loading: (a) $\omega = 0.00\%$, (b) $\omega = 2.01\%$, (c) $\omega = 2.23\%$, (d) $\omega = 2.40\%$, (e) $\omega = 2.49\%$, (f) $\omega = 2.53\%$, and (g) $\omega = 2.58\%$.

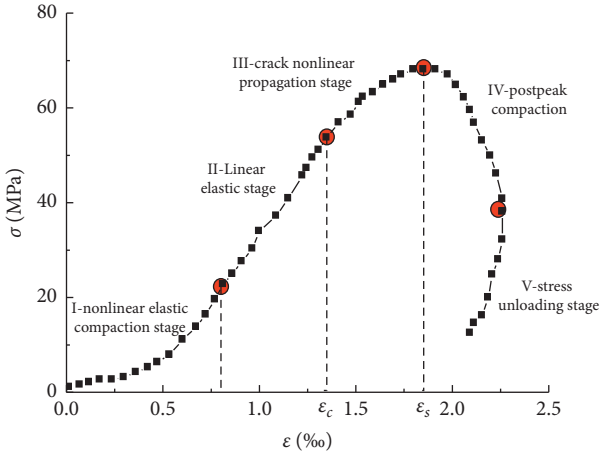

Figure 6: Typical stress-strain curve under dynamic test ($\omega = 2.53\%$, sample-2). ε_c and ε_s are strains at yielding strength and peak strength, respectively.

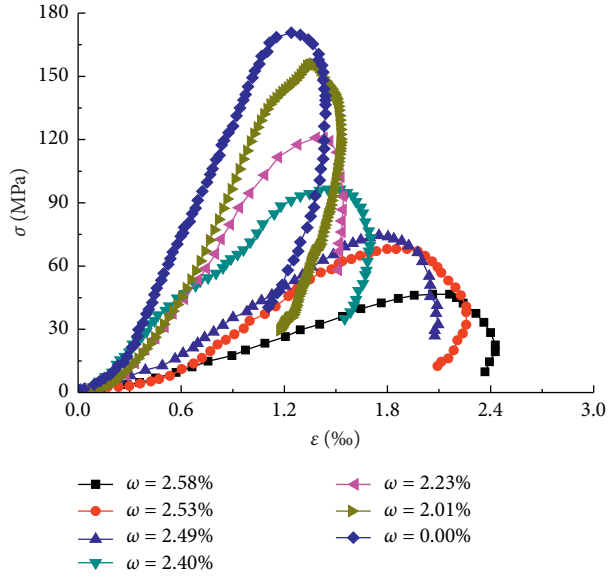

Figure 7: Stress-strain curves of sandstone with different moisture contents under dynamic loading.

Table 2 and Figure 8 show that with the gradual increase of moisture content, the average dynamic elastic modulus decreased approximately linearly, and the slope was 2495.22. For example, when the moisture content increases from 2.23% to 2.49%, the elastic modulus decreased by 5.84 GPa with a decrease percentage of 49.12%. When the moisture content increased from 2.49% to 2.58%, the elastic modulus decreased by 3.25 GPa with a decrease percentage of 53.72%. When the moisture content of the sample was increased from the dry state to 2.01%, the elastic modulus was only reduced by 0.25 MPa. The above data show that the rock impact resistance was closely associated with the moisture content. When the moisture content of the sample was less than 2.01%, the effect on the deformation resistance was slight, and vice versa.

3.3. Effect of Moisture Content on the Dynamic Peak Strength of Sandstone. Figure 9 shows the relationship between the peak strength of the sandstone sample and the moisture content. The average dynamic peak strength exhibited a nonlinear decrease as the moisture content increased, and the decrease rate gradually increased. For example, when the moisture content increased from 2.23% to 2.40%, the peak strength decreased by 18.05 MPa with a decrease percentage of 15.06%. When the moisture content increased from 2.53% to 2.58%, the peak strength decreased by 21.26 MPa with a decrease percentage of 31.22%. In addition, when the moisture content reached 2.49%, the peak strength of the

Table 2: Effect of moisture content on dynamic peak strain, dynamic peak strength, and dynamic elastic modulus.

Specimen	ω (%)	ε_d (‰)		σ_d (MPa)		E_d (GPa)	
		Sample	Average	Sample	Average	Sample	Average
1		1.24		170.72		18.03	
2	0.00	1.35	1.23	165.89	167.94	16.37	18.03
3		1.11		167.22		19.7	
1		1.29		143.37		15.25	
2	2.01	1.35	1.32	155.98	150.16	18.11	17.78
3		1.33		151.13		19.97	
1		1.36		122.09		13.59	
2	2.23	1.43	1.4	120.82	119.82	12.03	11.89
3		1.42		116.56		10.06	
1		1.45		96.44		7.37	
2	2.40	1.41	1.49	99.65	101.77	8.72	8.48
3		1.61		109.23		9.34	
1		1.78		81.43		6.33	
2	2.49	1.66	1.73	83.1	79.67	6.57	6.05
3		1.75		74.49		5.26	
1		1.83		64.89		4.86	
2	2.53	1.84	1.84	68.1	68.10	5.67	5.18
3		1.89		71.3		5.01	
1		2.02		45.07		2.72	
2	2.58	2.06	2.08	46.66	46.84	2.74	2.80
3		2.16		48.8		2.95	

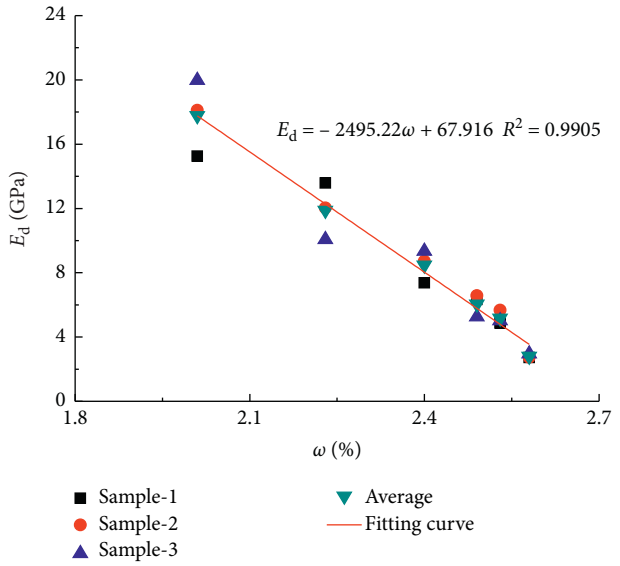

Figure 8: Dynamic elastic modulus variation with moisture content.

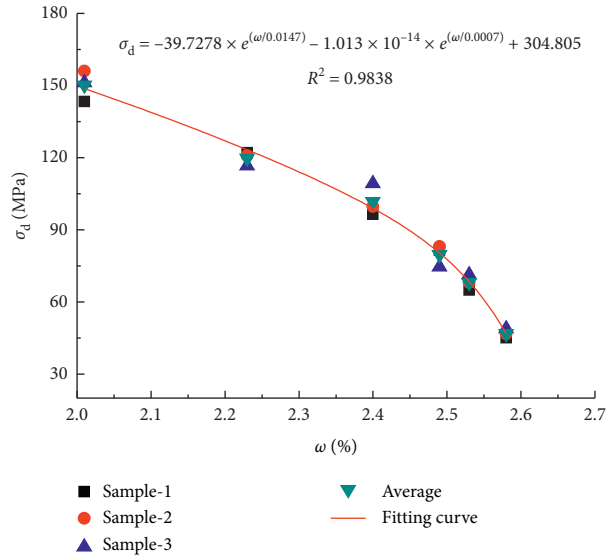

Figure 9: Dependence of peak strength on moisture content.

sample began to decrease sharply (Figure 10), indicating that the moisture content was a critical value for weakening the dynamic strength of the sandstone sample. As the moisture content continued to increase, its dynamic strength would drop sharply, promoting the occurrence possibility of dynamic disasters.

3.4. Effect of Moisture Content on the Dynamic Peak Strain of Sandstone. The peak strain reflected the degree of rock ductility, and the variation of peak strain with moisture content is shown in Figure 10. As the moisture content of the sample increased gradually, the peak strain increased nonlinearly and the increase rate gradually increased. For example, when the moisture content increased from 2.01% to 2.40%, the peak strain increased by 0.17‰ with an increase percentage of 12.88%. When the moisture content increased from 2.40% to 2.53%, the peak strain increased by 0.35‰ with an increase percentage of 23.49%. Compared with the dry condition, when the moisture content was 2.01%, the peak strain was slightly increased by 0.09 ‰. The above analysis showed that the moisture content had an important influence on the peak strain of sandstone. With the increase of moisture content, the ductility of the sample increased gradually, and it transited from brittle state to

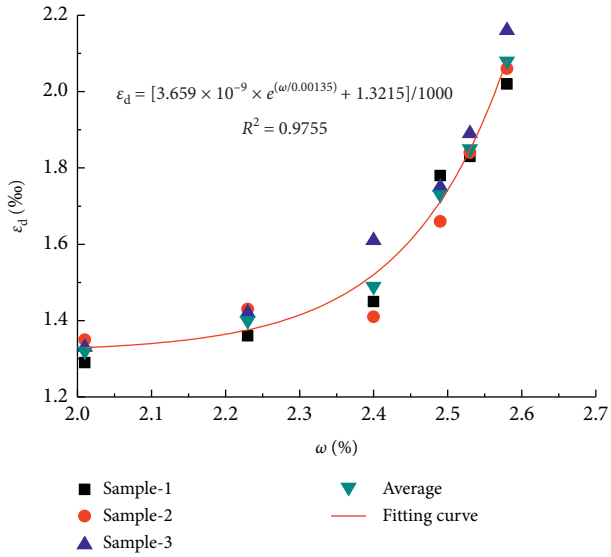

Figure 10: Dependence of peak strain on moisture content.

ductile state. Moreover, when the moisture content arrived 2.40%, the peak strain of the sample began to increase gradually, indicating that the moisture content was possibly a critical value of the brittle-ductile transition of the sandstone sample.

4. Evolution of Dynamic Brittle-Ductile Transition of Sandstone

4.1. Definition of the Dynamic Ductility Coefficient of Sandstone. Both brittleness and ductility were basic properties of rock material. The brittle failure occurred with no obvious plastic deformation before its peak strength. Conversely, it was called ductile failure with significant plastic deformation. In fact, the brittle-ductility behavior of rocks was not only related to its stress state but also closely related with its moisture content and temperature (Fujimoto [12]; Zhu [13]; Kim [20]; Nicolas [11]). Microscopically, the brittle-ductile transition of rock was mainly reflected by the transition of brittle fracture of local structure to crystal plastic deformation. Quantitative description of the brittle-ductile transition of rock was presented by the brittle-ductility coefficient. The commonly used definitions of the brittle-ductility coefficient were all proposed under static load conditions (Kahraman [24], Zhang [28], and Tarasov [27]), which were not necessarily applicable to dynamic load conditions. To accurately reflect the influence of moisture content on dynamic brittle-ductile transition of sandstone, we used the ratio between the peak strain and the yield strain to reflect the degree of brittle-ductility transition, which was termed the dynamic ductility coefficient (η):

$$\eta = \frac{\varepsilon_s}{\varepsilon_c}. \quad (5)$$

4.2. Relationship between Dynamic Ductility Coefficient and Moisture Content. According to equation (5), the dynamic ductility coefficient of each sample with different moisture contents is shown in Table 3. The variation of dynamic ductility coefficient of sandstone with different moisture contents is shown in Figure 11. The dynamic ductility coefficient of the dry sandstone was 1.147. When the moisture content reached 2.23%, the ductility coefficients were only increased by 1.13% compared with the dry state, indicating that when the moisture content of the sample was lower than 2.23%, the dynamic failure characteristics were basically the same as the dry state. When the moisture content increased from 2.23% to 2.58%, the dynamic ductility coefficient of the sample showed a significant nonlinear increase, and the increase rate gradually increased. Particularly, when the moisture content reached 2.40% to 2.49%, the growing rate increased significantly. The above analysis showed that the moisture content had a significant effect on the brittle-ductility transition of the sample. There was a significant interval effect, that was, when the moisture content was lower than 2.23% and the dynamic ductility coefficient was small, and the sample mainly failed in brittle. When it reached 2.23%, the dynamic ductility coefficient started to increase nonlinearly, but the value was still small, which the failure mode may be in the form of brittle-ductile composite. When the moisture content was in the range of 2.40%~2.58%, the dynamic ductility coefficient was larger, and the increase rate was appreciable. The sample may be dominated by ductile damage.

4.3. Microfracture Morphology of Sandstone with Different Moisture Contents. When the moisture content was low, the sandstone displayed brittle fracture. When the moisture content exceeds a certain range, the sandstone was mainly in ductile fracture. To further reveal the effect of moisture content on the brittle-ductile transition of sandstone microscopically, the scanning electron microscopy (SEM) was used to scan the fracture morphology of sandstone with different moisture contents after the dynamic test.

4.3.1. Experimental Apparatus and Sample Preparation. The TESCAN VEGA scanning electron microscope (SEM) used in this study mainly included electron beam system, scanning system, signal test amplification system, image display and recording system, and vacuum system (Figure 12). The electron beam system consisted of an electron gun and an electromagnetic lens. It was mainly used to generate an electron beam with a certain energy acting on the sample surface. The vacuum system mainly included a vacuum pump and a vacuum column. The test sample was selected from the broken pieces after the impact test. The sample preparation procedures were as follows. First, the broken piece with smooth surface of the fracture surface was selected as the test sample. The selected sample was prepared into a diameter of about 10 mm that approximates the coin size. Then, the sample was bonded to the bonding table, and the fine particles and dust on the sample surface were blown off. Afterwards, the sample was dried and gold-plated. Finally, the sample was placed under SEM. The surface fracture morphology was observed by magnifying 500 times, 2000

Table 3: Dynamic ductility coefficient of sandstone under different moisture contents.

Sample	$\omega = 0.00\%$	$\omega = 2.01\%$	$\omega = 2.23\%$	$\omega = 2.40\%$	$\omega = 2.49\%$	$\omega = 2.53\%$	$\omega = 2.58\%$
1#	1.159	1.122	1.162	1.160	1.20	1.204	1.217
2#	1.125	1.184	1.172	1.156	1.19	1.195	1.191
3#	1.156	1.147	1.145	1.238	1.18	1.204	1.325
Average	1.147	1.151	1.16	1.185	1.190	1.201	1.244

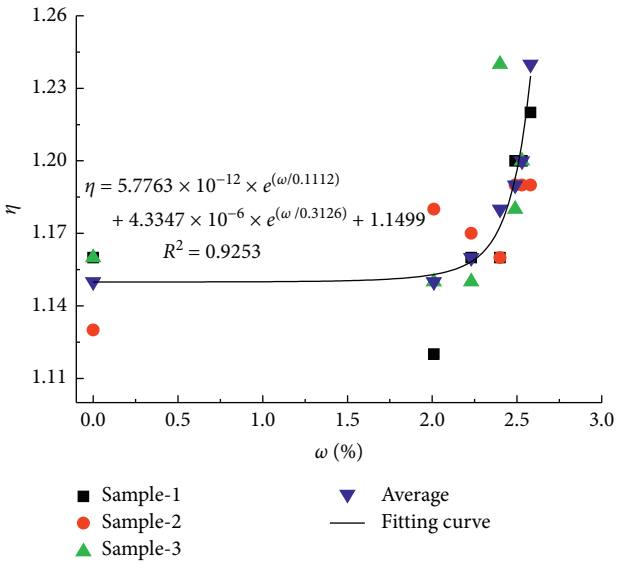

Figure 11: Effect of moisture content on the dynamic ductility coefficient.

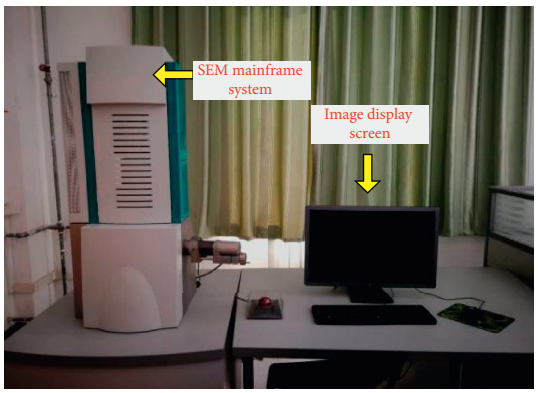

Figure 12: TESCAN VEGA scanning electron microscope (SEM).

times, and 5000 times, respectively, and the fracture characteristics were analyzed.

4.3.2. Effect of Moisture Content on Microfracture Morphology of Sandstone

(1) Description of Fracture Morphology. According to the fractography, Bahat [34] and Zhong [35] have summarized the typical fracture morphology of rock material through a series of experimental research studies and some research results are shown in Table 4.

Because the sandstone specimen belonged to a polycrystalline material arranged in disorder, when the cleavage propagates through one particle to the neighboring particles, the cleavage cracks would be generated on different crystal surfaces. These cleavage cracks intersected to form steps and looked like rivers on earth under SEM. Therefore, they were called river pattern. As shown in Figure 13, most of these patterns originated from the boundary of particles, and their direction of expansion could also be determined according to the pattern shape (Zuo [36]). Generally, the step pattern would be formed by the tearing action of two cleavage cracks which were not in the same plane. From Figures 13–15, it showed that the height and size of the step pattern varied from a few microns to 20 microns, which may be related to rock properties and moisture content. As a form of ductile failure, the dimple pattern mainly exhibited the local plastic deformation of sandstone specimen, which would be formed when the movement of mineral particles within the rock was restricted by adjacent particles under external loads (Cui [37]). In addition, the slip step pattern and snake slippery pattern showed significant signs of slippage and would be formed when shear sliding failure occurred during the test. However, both sides of snake slippery pattern exhibited relatively smooth (see Figures 13(e) and 15(c)) and the slip step pattern consisted of several uneven steps (see Figures 13(d), 14(d), and 15(d)). Based on the above statement, the effect of moisture content on the brittle-ductile transition of sandstone specimen could be analyzed as follows.

(2) Analysis of Fracture Morphology under Different SEM Magnifications. Figures 13–15 exhibit the microstructure of sandstone at the magnification of 500, 2000, and 5000 times with different moisture contents, respectively. From Figures 13–15, it indicated that the fracture morphologies of sandstone in dry state and 2.01% moisture content were mainly dominated by step pattern and river pattern at any magnification. Hence, the overall failure mode belonged to typical brittle fracture.

For 500 times magnification, when the moisture content was in the range of 2.23%~2.40%, a smooth cleavage step pattern was observed, and a clear river pattern was distributed in the upper or lower part of the SEM image. Some river patterns extend in the direction same as the cleavage step pattern. So, the overall failure mode was obvious brittle fracture. When the moisture content was in the range of 2.49%~2.58%, a large number of dimple patterns (see Figures 13(e)–13(g)) and snake slippery patterns (see Figure 13(e)) were distributed in the SEM image. With increasing moisture content, the dimple pattern gradually

Table 4: Typical fracture morphology of rock material.

Fracture mode	Pattern type
Brittle (tensile) fracture	River pattern, step pattern, fishbone pattern, intergranular crack, root pattern, scaly pattern, etc.
Ductile (shear) fracture	Parallel sliding pattern, snake slippery pattern, trans crystalline cracking, flat pattern, tetrahedral pattern, dimple pattern, slip step pattern, etc.

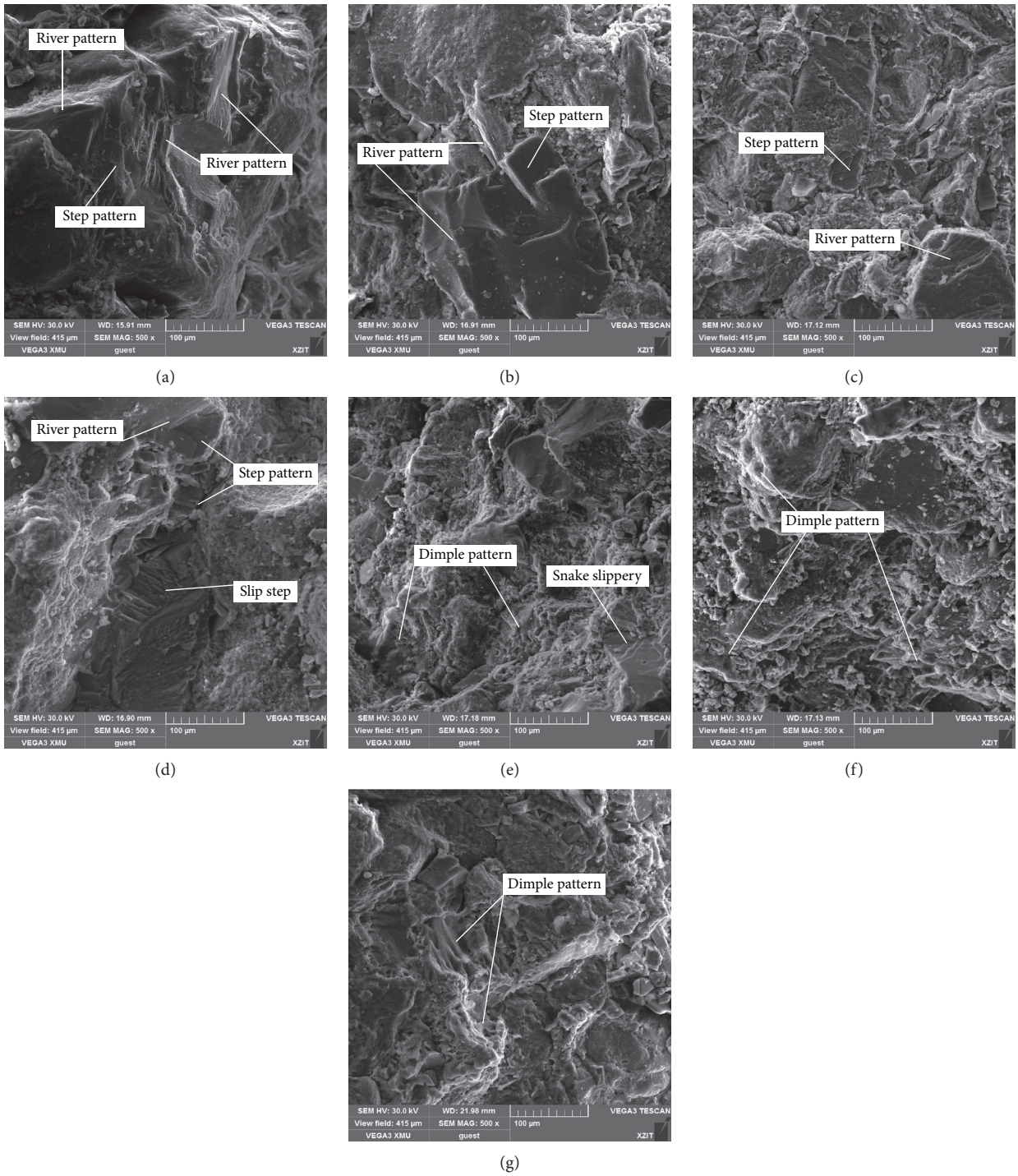

Figure 13: Sandstone fracture morphology with different moisture contents at 500 times magnification: (a) $\omega = 0\%$, (b) $\omega = 2.01\%$, (c) $\omega = 2.23\%$, (d) $\omega = 2.40\%$, (e) $\omega = 2.49\%$, (f) $\omega = 2.53\%$, and (g) $\omega = 2.58\%$.

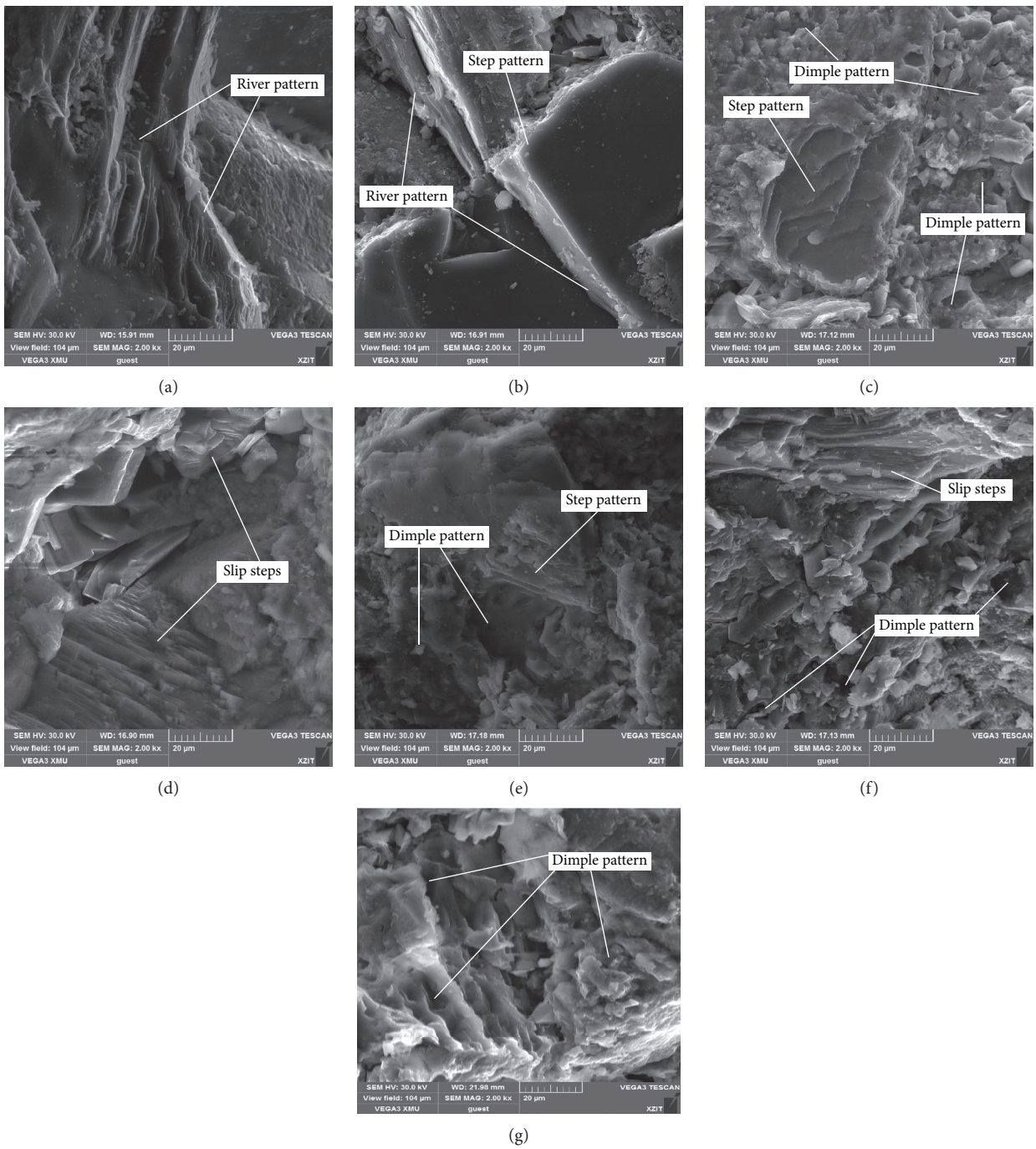

Figure 14: Sandstone fracture morphology with different moisture contents at 2000 times magnification: (a) $\omega = 0\%$, (b) $\omega = 2.01\%$, (c) $\omega = 2.23\%$, (d) $\omega = 2.40\%$, (e) $\omega = 2.49\%$, (f) $\omega = 2.53\%$, and (g) $\omega = 2.58\%$.

changed from isolated state to interconnected states with the appearance of local dimple clusters. Meanwhile, the maximin size of the dimple patterns also slightly increased from 0–10 μm at $\omega = 2.49\%$ to 0–35 μm at $\omega = 2.58\%$. In addition, the dimple pattern of $\omega = 2.58\%$ differed from those of $\omega = 2.49\%$ and $\omega = 2.53\%$. They were mainly elongated dimples connected to each other. Based on the above analysis, when the moisture content varied from 2.49% to 2.58%, the failure mode was mainly dominated by ductile fracture.

The brittle-ductile transition of the sandstone sample was complicated, which was difficult to fully understand at a low magnification. Therefore, it was necessary to study the effect of moisture content on the microstructure of sandstone sample at the magnification of 2000 and 5000 times.

As shown in Figures 14 and 15, when the moisture content reached 2.23%, the fracture morphology displayed step pattern (Figures 14(c) and 15(c)), snake slippery pattern (Figure 15(c)), and a small amount of dimple patterns (Figure 14(c)). Although the step pattern exhibited certain

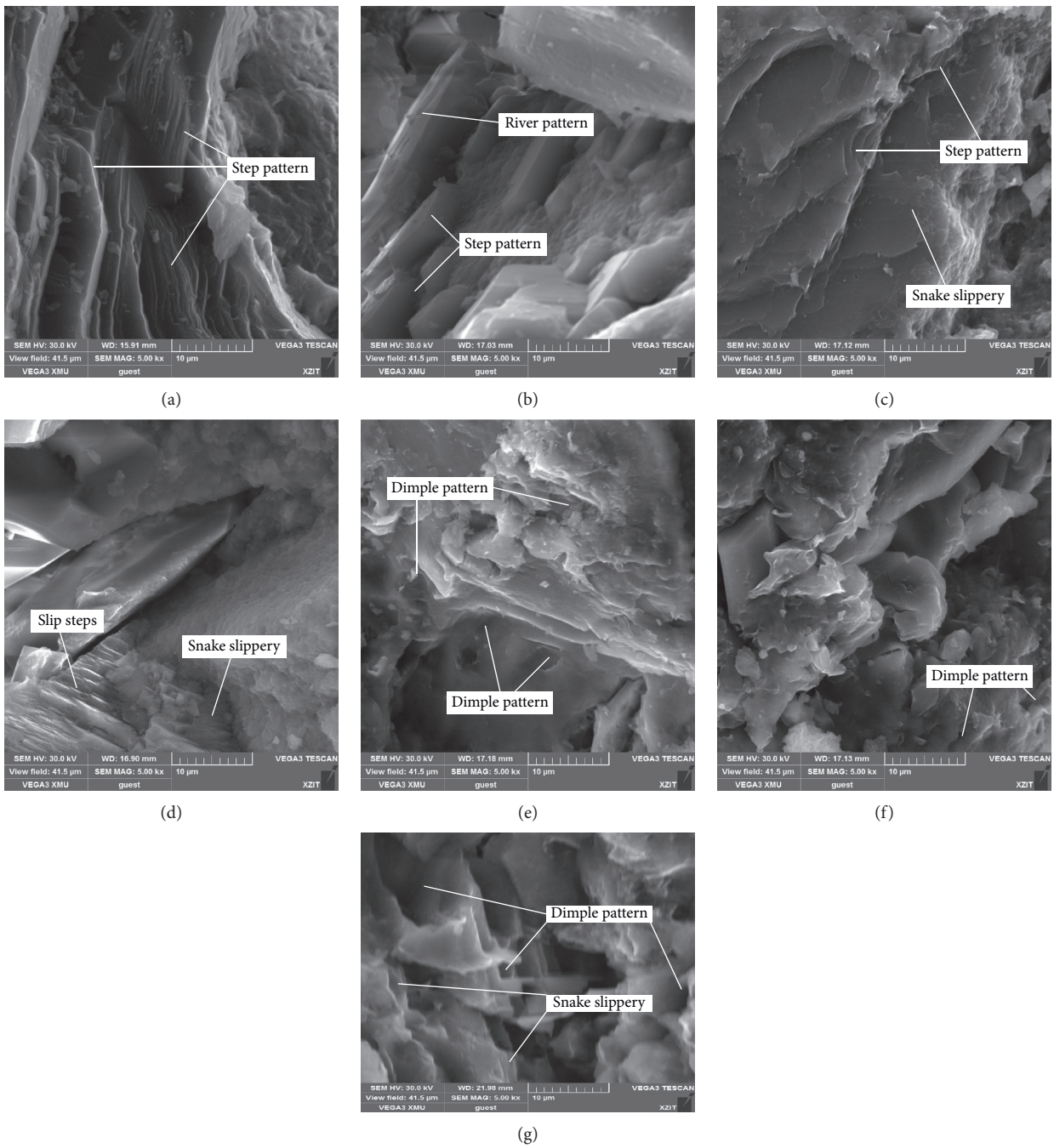

Figure 15: Sandstone fracture morphology with different moisture contents at 5000 times magnification: (a) $\omega = 0\%$, (b) $\omega = 2.01\%$, (c) $\omega = 2.23\%$, (d) $\omega = 2.40\%$, (e) $\omega = 2.49\%$, (f) $\omega = 2.53\%$, and (g) $\omega = 2.58\%$.

slip, it was not obvious at 2000 times and 5000 times magnification. Meanwhile, both the number and the size of dimple pattern and snake slippery pattern were small, most of which were in the developing stage. Thus, the fracture mode was still dominated by brittle fracture with the localized ductile fracture. When the moisture content was 2.40%, the fracture morphology was mainly shear-slip step, with black lines distributed between adjacent steps. These black lines are shear slip zone composed of a large number of sliding steps. The snake slippery pattern and trans crystalline cracking (Figure 15(d)) were also clearly observed at 5000 times magnification. Hence, the fracture mode could be characterized by ductile fracture (Zhang [28]). When the moisture content was in the range of 2.49%~2.58%, a large area of dimple clusters could be observed in SEM image, and the inner walls of dimple pattern showed signs of slippage. With the increase of moisture content, the dimple clusters were gradually transited from isolated state to interconnected state. For 2000 times magnification, when the moisture content reached 2.49% and 2.53%, the fracture

mode also exhibited a large number of slip step patterns (Figure 14(f)), and a number of sliding steps were distributed between adjacent steps where the sliding steps were formulated. For 5000 times magnification, when moisture content reached 2.58%, the snake slippery pattern (Figure 15(g)) could be clearly observed in SEM image and the dimple pattern alternate with snake slippery patterns. It means that the shear failure played a leading role in this region. Hence, when the moisture content was in the range of 2.49%~2.58%, the sandstone failure mode was mainly ductile fracture, which was consistent with the analysis results at 500 times magnification.

Based on the above analysis, it indicated that the result obtained by SEM image was consistent with the analysis of the dynamic ductility coefficient in Section 4.2, which established the relationship between macroscopic parameters and microscopic analysis. Therefore, the dynamic ductility coefficient could effectively reflect the influence of moisture content on the brittle-ductility transition of sandstone specimen.

5. Discussion

Natural rock was composed of various types of mineral crystal particles. Many defects such as primary pores and fissures were inside the sample (Kim [20]). Water entered the sample pores through capillary action. When the adhesion between the crystals was gradually weakened, the brittleness was reduced, and the plasticity was enhanced, leading to the increase of ductility (Liu [16]). Meanwhile, the higher the moisture content of the sample, the larger the influential region on the internal crystal structure bonding (Nicolas [11] and Wasantha [7]). Thus, the weakening degree of the bonding between the crystals was higher, and the ductility was enhanced. From the microstructure of rock mass, rock damage caused by water could be mainly reflected by pattern types. The ductile failure was mainly related to shear failure, which could be deduced by dimple pattern, snake slippery pattern, slip step pattern, etc. (Zuo [36]). From Figures 13–15, it can be seen clearly that those patterns gradually increased with increasing moisture content. It means that the shear failure gradually dominated the mode of specimen failure with increasing moisture content, which reflected that moisture content had a significant role in promoting the brittleness-ductility transition of sandstone.

6. Conclusions

In this paper, the dynamic mechanical properties of sandstone with different moisture contents were studied using the SHPB test system under the same strain rate. How the moisture content affected the dynamic mechanical properties of sandstone was explored. A dynamic ductility coefficient was proposed to quantify the dependence of brittle-ductile transition of sandstone on moisture content. Through SEM technique, the microstructure of sandstone samples under different moisture contents was analyzed with the magnification of 500 times, 2000 times, and 5000 times, respectively. The impact of moisture content on the dynamic brittle-ductile transition of sandstone was revealed. The following conclusions are summarized:

(1) Moisture content had a considerable effect on the stress-strain curves of sandstone. The curve could be divided into dynamic nonlinear elastic compression stage, linear elastic stage, crack nonlinear expansion stage, postpeak compression stage, and stress unloading stage. As the moisture content gradually increased, the nonlinear elastic compression stage of the sample increased. The dynamic compression stage of the dry sample was the shortest.

(2) With increasing moisture content, the dynamic peak strength and elastic modulus of sandstone decreased to different extents, whereas the dynamic peak strain increased nonlinearly. The moisture content had a significant influence on the dynamic ductility coefficient of the sample with obvious interval effect. With the increase of moisture content, the ductility coefficient of the sample exhibited a nonlinear increase. When the moisture content was lower than 2.23%, the dynamic ductility coefficient was small, and the sample failure model was mainly brittle fracture. When it reached 2.23%, the increasing rate of the dynamic ductility coefficient began to increase slightly, and the sample mainly consisted of brittle-ductile composite failure. When it ranged from 2.40% to 2.58%, the sample mainly exhibited ductile failure.

(3) Based on the SEM examination, when the magnification was 500 times, the microstructure of sandstone samples with dry state and moisture contents varying from 2.01% to 2.40% was mainly composed of step pattern and river pattern, which belonged to brittle fracture. When the moisture content was in the range of 2.49%~2.58%, the microstructure of the sample exhibited a large number of dimple clusters in different sizes with regional snake patterns. And the failure mainly exhibited ductile fracture. For 2000 times and 5000 times magnification, the microstructure of the sample with moisture content lower than 2.23% displayed mainly brittle fracture, and the microstructure of the sample with moisture content of 2.23% exhibited brittle-ductile composite fracture. Other samples exhibited ductile fracture, which was generally consistent with the results reflected by the dynamic ductility coefficient, which in turn verified the accuracy of the macroscopic parameter.

(4) The water injection into rock stratum was one of the most effectively ways to reduce rock bursts. The macroscopic parameter (dynamic ductility coefficient) could effectively reveal the influence of moisture content on brittle-ductility transition of rock materials. This research result had a guiding significance for revealing the mechanism of water mitigating the occurrence of rock burst.

Data Availability

The data of the pictures and tables used to support the findings of this study are included within the article.

Conflicts of Interest

The authors declare that they have no conflicts of interest.

Acknowledgments

The authors gratefully acknowledge the financial support of Coal Joint Fund Incubation Project (U1710120) and National Natural Science Foundation (51704281).

References

[1] R. M. Iverson, "Landslide triggering by rain infiltration," *Water Resources Research*, vol. 36, no. 7, pp. 1897–1910, 2000.

[2] H. Bai, D. Ma, and Z. Chen, "Mechanical behavior of groundwater seepage in karst collapse pillars," *Engineering Geology*, vol. 164, pp. 101–106, 2016.

[3] T. Lu, Z. Zhao, and H. Hu, "Improving the gate road development rate and reducing outburst occurrences using the waterjet technique in high gas content outburst-prone soft coal seam," *International Journal of Rock Mechanics and Mining Sciences*, vol. 48, no. 8, pp. 1271–1282, 2011.

[4] D. Song, E. Wang, Z. Liu et al., "Numerical simulation of rockburst relief and prevention by water-jet cutting," *International Journal of Rock Mechanics & Mining Sciences*, vol. 70, no. 9, pp. 318–331, 2017.

[5] C. Zhang, I. Canbulat, B. Hebblewhite, and C. R. Ward, "Assessing coal burst phenomena in mining and insights into directions for future research," *International Journal of Coal Geology*, vol. 179, pp. 28–44, 2017.

[6] Y. Zhao, S. Gong, C. Zhang, Z. Zhang, and Y. Jiang, "Fractal characteristics of crack propagation in coal under impact loading," *Fractals*, vol. 26, no. 2, Article ID 1840014, 2018.

[7] P. L. P. Wasantha and P. G. Ranjith, "Water-weakening behavior of Hawkesbury sandstone in brittle regime," *Engineering Geology*, vol. 178, no. 8, pp. 91–101, 2017.

[8] Y. B. Zhang, C. P. Liu, P. Liang et al., "Experimental study on the impact of water on rock compressive strength," *International Forum on Energy, Environment Science and Materials (IFEESM)*, vol. 40, pp. 58–62, 2018.

[9] P. Baud, W. Zhu, and T.-f. Wong, "Failure mode and weakening effect of water on sandstone," *Journal of Geophysical Research: Solid Earth*, vol. 105, no. B7, pp. 16371–16389, 2000.

[10] X. J. Liu, C. Yang, and J. Yu, "The influence of moisture content on the time-dependent characteristics of rock material and its application to the construction of a tunnel portal," *Advances in Materials Science and Engineering*, vol. 12, pp. 405–418, 2015.

[11] A. Nicolas, J. Fortin, J. B. Regnet, A. Dimanov, and Y. Guéguen, "Brittle and semibrittle behaviours of a carbonate rock: influence of water and temperature," *Geophysical Journal International*, vol. 206, no. 1, pp. 438–456, 2016.

[12] K. Fujimoto, T. Ohtani, N. Shigematsu et al., "Water-rock interaction observed in the brittle-plastic transition zone," *Earth, Planets and Space*, vol. 54, no. 11, pp. 1127–1132, 2002.

[13] W. Miyashita, X. Xiao, and B. Evans, *The Brittle-Ductile Transition in Fine-Grained Carbonate Rocks: Effect of Water*, AGU Fall Meeting, New Orleans, LA, USA, 2006.

[14] L. Han, Y. Zhou, and H. Li, *Fault Weakening by Water in the Brittle-Plastic Transition Zone of the Wenchuan Fault Zone (Longmenshan, China): A Study Through Deformed Exhumed Granites*, AGU Fall Meeting, New Orleans, LA, USA, 2012.

[15] J. Suppe, *Role of Fluid Overpressures in Crustal Strength and the form of the Brittle-Ductile Transition*, AGU Fall Meeting, New Orleans, LA, USA, 2014.

[16] Z. Liu and J. Shao, "Moisture effects on damage and failure of Bure claystone under compression," *Géotechnique Letters*, vol. 6, no. 3, pp. 182–186, 2016.

[17] L. N. Y. Wong, V. Maruvanchery, and G. Liu, "Water effects on rock strength and stiffness degradation," *Acta Geotechnica*, vol. 11, no. 4, pp. 716–737, 2016.

[18] E. H. Kim, O. De, and B. M. Davi, "The effects of water saturation on dynamic mechanical properties in red and buff sandstones having different porosities studied with split Hopkinson pressure bar (SHPB)," *Applied Mechanics & Materials*, vol. 752-753, pp. 784–789, 2018.

[19] Z. Zhou, X. Cai, W. Cao, X. Li, and C. Xiong, "Influence of water content on mechanical properties of rock in both saturation and drying processes," *Rock Mechanics and Rock Engineering*, vol. 49, no. 8, pp. 3009–3025, 2016.

[20] E. Kim and H. Changani, "Effect of water saturation and loading rate on the mechanical properties of Red and Buff Sandstones," *International Journal of Rock Mechanics and Mining Sciences*, vol. 88, pp. 23–28, 2016.

[21] T.-f. Wong and P. Baud, "The brittle-ductile transition in porous rock: a review," *Journal of Structural Geology*, vol. 44, no. Complete, pp. 25–53, 2012.

[22] S. Kahraman, "Correlation of TBM and drilling machine performances with rock brittleness," *Engineering Geology*, vol. 65, no. 4, pp. 269–283, 2002.

[23] R. Altindag, "Correlation of specific energy with rock brittleness concepts on rock cutting," *Journal of the Southern African Institute of Mining and Metallurgy*, vol. 103, no. 3, pp. 163–171, 2003.

[24] S. Kahraman and R. Altindag, "A brittleness index to estimate fracture toughness," *International Journal of Rock Mechanics and Mining Sciences*, vol. 2, no. 41, pp. 343–348, 2004.

[25] Q. M. Gong and J. Zhao, "Influence of rock brittleness on TBM penetration rate in Singapore granite," *Tunnelling and Underground Space Technology*, vol. 22, no. 3, pp. 317–324, 2007.

[26] B. G. Tarasov and M. F. Randolph, "Superbrittleness of rocks and earthquake activity," *International Journal of Rock Mechanics and Mining Sciences*, vol. 48, no. 6, pp. 888–898, 2011.

[27] B. Tarasov and Y. Potvin, "Universal criteria for rock brittleness estimation under triaxial compression," *International Journal of Rock Mechanics and Mining Sciences*, vol. 59, pp. 57–69, 2013.

[28] L. Y. Zhang, *Damage evolution and fracture mechanism of mudstone under high temperature*, Ph.D. Thesis, China University of Mining and Technology, Xuzhou, China, 2012.

[29] F. J. Cooper, J. P. Platt, and W. M. Behr, "Rheological transitions in the middle crust: insights from cordilleran metamorphic core complexes," *Solid Earth*, vol. 8, no. 1, pp. 199–215, 2017.

[30] Y. S. Zhou, C. R. He, and H. Yang, "The effect of water on brittle-plastic transition of lower crustal mafic rocks," *Seismology & Geology*, vol. 26, no. 3, pp. 472–483, 2004.

[31] Q. Ma, D. Ma, and Z. Yao, "Influence of freeze-thaw cycles on dynamic compressive strength and energy distribution of soft rock specimen," *Cold Regions Science and Technology*, vol. 153, pp. 10–17, 2018.

[32] Y. S. Yan and X. W. Chen, "The effect of impulse shaper on the SHPB waves," *Journal of Southwest University of Science and Technology*, vol. 28, no. 1, pp. 36–42, 2013.
[33] M. Li, X. Mao, H. Pu, Y. Chen, and Y. Wu, "Effects of heating rate on the dynamic tensile mechanical properties of coal sandstone during thermal treatment," *Shock and Vibration*, vol. 2017, no. 8, 11 pages, Article ID 4137805, 2017.
[34] D. Zhang, *Tectonofractography*, Springer, Berlin, Germany, pp. 239–324, 1991.
[35] Q. Zhong and Z. Zhao, *Fractography*, Higher Education Press, Beijing, China, 2006.
[36] J. Zuo, H. Xie, H. Zhou, Y. Fang, and X. Fan, "Fractography of sandstone failure under temperature-tensile stress coupling effects," *Chinese Journal of Rock Mechanics and Engineering*, vol. 26, no. 12, pp. 2444–2457, 2007.
[37] Y. Cui and C. Wang, *Analysis of Metal fracture*, Harbin Institute of Technology Press, Harbin, 1998, in Chinese.